

## **Modeling of the Hemodynamic Responses in Block Design fMRI Studies**

Zuyao Y Shan<sup>1</sup>, Margaret J Wright<sup>2</sup>, Paul M Thompson<sup>3</sup>, Katie L McMahon<sup>1</sup>, Gabriella G A M Blokland<sup>2</sup>, Greig I de Zubicaray<sup>4</sup>, Nicholas G Martin<sup>2</sup>, Anna AE Vinkhuyzen<sup>5</sup>, David C Reutens<sup>1</sup>

<sup>1</sup>Centre for Advanced Imaging, The University of Queensland, Brisbane, QLD 4072, Australia; <sup>2</sup>Queensland Institute of Medical Research, Brisbane, QLD 4029, Australia; <sup>3</sup>Imaging Genetics Center, Laboratory of Neuro Imaging, Department of Neurology & Psychiatry, UCLA School of Medicine, Los Angeles, CA, United States; <sup>4</sup>School of Psychology, The University of Queensland, Brisbane, QLD 4072, Australia; <sup>5</sup>Queensland Brain Institute, The University of Queensland, Brisbane, QLD 4072, Australia

**Correspondence:** Zuyao Shan, PhD  
Centre for Advanced Imaging  
University of Queensland  
Brisbane St Lucia, QLD 4072, Australia  
Telephone: +61-7-334-69026  
E-mail: [zuyao.shan@cai.uq.edu.au](mailto:zuyao.shan@cai.uq.edu.au)

**Short Title:** Hemodynamic Response Modeling and its Reliability

**Disclosure/Conflict of Interest:** The authors declare no conflict of interest

**Abstract**

The hemodynamic response function (HRF) describes the local response of brain vasculature to functional activation. Accurate HRF modeling enables the investigation of cerebral blood flow regulation and improves our ability to interpret fMRI results. Block designs have been used extensively as fMRI paradigms because detection power is maximized; however, block designs are not optimal for HRF parameter estimation. Here we assessed the utility of block design fMRI data for HRF modeling. The trueness (relative deviation), precision (relative uncertainty), and identifiability (goodness-of-fit) of different HRF models were examined and test-retest reproducibility of HRF parameter estimates for a commonly used block design paradigm was assessed using computer simulations and fMRI data from 82 healthy young adult twins (mean age 22.5 year old), acquired on two occasions 3-4 months apart. The effects of systematically varying attributes of the block design paradigm were also examined. In our comparison of five HRF models, the model comprising the sum of two gamma functions with six free parameters had greatest parameter accuracy and identifiability. HRF height and time-to-peak were highly reproducible between studies and width was moderately reproducible but the reproducibility of onset time was low. This study established the feasibility and test-retest reliability of estimating HRF parameters using data from block design fMRI studies.

**Key Words:** fMRI, Hemodynamic Response, Hemodynamic Response Function (HRF), test-retest reliability,

## **Introduction**

The hemodynamic response function (HRF) reflects the regulation of regional cerebral blood flow in response to neuronal activation. Accurate modeling of the HRF is of interest in a number of areas of research.<sup>1-5</sup> The HRF plays a key role in the analysis of functional magnetic resonance imaging (fMRI) data<sup>3</sup> and variation in the HRF between individual subjects and between brain regions has prompted the estimation of subject-specific HRFs as a means of enhancing the accuracy and power of fMRI studies.<sup>1</sup> Characteristics of the shape of the evoked hemodynamic response such as height, delay, and duration may also be used to infer information about intensity, onset latency, and duration of the underlying neuronal activity.<sup>4</sup> Accurate estimation of the HRF is essential if fMRI is to be used to detect fine differences in the timing of neuronal activation as a means of understanding the temporal sequences of brain processes. HRF modeling also enables noninvasive investigation of neurovascular coupling which changes with brain aging and which may play a pathophysiological role in dementia and cerebrovascular disease.<sup>6,7</sup>

The design of fMRI studies affects both estimation efficiency, a measure of the ability to estimate the shape of the HRF, and detection power, a measure of the ability to detect activation. Previous studies have demonstrated that there is a fundamental tradeoff between these characteristics such that designs maximizing detection power necessarily have minimum estimation efficiency and designs that achieve maximum estimation efficiency cannot attain maximum detection power.<sup>8,9</sup> For example, randomized event-related designs offer high estimation efficiency but poor detection power, while block designs offer good detection power at the cost of low estimation efficiency.<sup>9</sup>

A considerable body of fMRI data has already been acquired using block designs to maximize signal-to-noise ratio and to increase the likelihood of detecting a response. In some of these studies, it would be of interest to examine the HRF explicitly even though study designs were not optimized with this in mind. In particular, studies involving large numbers of subjects,<sup>10, 11</sup> multiple sites,<sup>10, 12, 13</sup> special subject groups,<sup>11, 14</sup> and longitudinal designs<sup>14</sup> would be difficult and expensive to replicate. Our specific interest in estimating HRF parameters from a block design study was stimulated by a large twin study. Here we were interested in how robustly HRF parameters could be estimated as a prelude to examining the heritability of the hemodynamic response function. We approached this question firstly by comparing the performance of different HRF models. We then examined the test-retest reliability of HRF parameter estimation. This allowed us to identify which HRF traits remain stable over time, providing some insight into the extent to which individual parameters serve as variables reflecting a biological trait or an experimental state. Test-retest reliability was examined in 82 healthy young adult twins tested with the same fMRI paradigm on two occasions. We examined the following parameters of the HRF: height ( $H$ ), time to peak ( $T$ ), full width at half maximum ( $W$ ), and onset ( $O$ ), respectively reflecting the magnitude, peak latency, duration, and onset latency of the localized increase in blood flow with neural activation.

## **Method**

### *HRF model and features*

The blood oxygenation level dependent (BOLD) fMRI signal was modeled as the convolution of the stimulus function and the HRF. Before assessing test-retest reliability in human data, we assessed the identifiability of five HRF models,

summarized in Table 1, in simulated fMRI time series. Model I was the canonical HRF used in SPM8 (The Wellcome Trust Centre for Neuroimaging, London, UK), in which only the height parameter  $A$  varies. Models II, III, and IV were variants of the canonical HRF and comprise the sum of two or three gamma functions. Model V was the sum of inverse logit functions used by Lindquist et al.<sup>4, 15</sup> The number of free parameters for model V was reduced from nine (three inverse logit functions) to seven by explicitly imposing the conditions that the fitted response should start and end at zero<sup>4,15</sup> noting that the other models were implicitly constrained to the same condition by their equations. Models III and V were chosen because they were previously found to have low parameter bias for event-related designs.<sup>4</sup> Model IV was chosen as it can model the initial dip and post-stimulus undershoot.<sup>16</sup>

-----  
Table 1  
-----

We used the following summary HRF features: height ( $H$ ), defined as the maximum signal change during the peri-stimulus time window (30 seconds was used for this study); time to peak ( $T$ ), the time taken from start time to the time when signal change reached its maximum value; full width at half maximum of the HRF ( $W$ ); the onset ( $O$ ), the first time point following the stimulus at which signal intensity exceeded  $0.1 \times H$  (Figure 1a).

-----  
Figure 1  
-----

*Simulation of fMRI signal time course*

fMRI signal time courses were simulated using known HRFs to test the performance

of different HRF models. Three ground-truth HRFs were created (Figure S1). In Simulation 1, the HRF was generated using the balloon model.<sup>17, 18</sup> The HRF was generated using a single input at 1.5s with 0.1s duration and using typical parameters obtained empirically in a previous study: neuronal efficacy 0.54, signal decay 1.54, auto-regulation 2.46, transit time 0.98, stiffness parameter, 0.33, resting oxygen extraction, 0.34, and resting blood volume fraction, 0.06.<sup>18</sup> The HRF in Simulation 2 was generated using the sum of four inverse logit functions to create four segments of HRF time course:

$$h(t) = \sum_{i=1}^4 A_i \frac{1}{1 + e^{(t-T_i)/D_i}}, \quad (6)$$

in which  $A_1 = -0.2$ ,  $A_2 = 1.8$ ,  $A_3 = -1.8$ ,  $A_4 = 0.2$ ,  $T_1 = 0.1$ ,  $T_2 = 4$ ,  $T_3 = 10$ ,  $T_4 = 20$ ,  $D_1 = 0.8$ ,  $D_2 = 1$ ,  $D_2 = 1$  and  $D_3 = 1.2$ . These parameters were determined empirically as generating an HRF shape with summary features ( $H$ ,  $W$ ,  $T$ , and  $O$ ) in keeping with published values.<sup>19, 20</sup> In Simulation 3, we used the sum of three gamma functions to generate the HRF:

$$h(t) = \sum_{i=1}^3 \left( A_i \frac{t^{\alpha_i-1} \beta_i^{\alpha_i} e^{-\beta_i t}}{\Gamma(\alpha_i)} \right) \quad (7),$$

in which  $A_1 = -0.2$ ,  $A_2 = 10$ ,  $A_3 = -3.6$ ,  $\alpha_1 = 1.5$ ,  $\alpha_2 = 6.6$ ,  $\alpha_3 = 15$ ,  $\beta_1 = 0.8$ ,  $\beta_2 = 0.8$ , and  $\beta_3 = 1$ . Figure 1 illustrates the procedures we used to simulate the fMRI time series. We used a block design stimulus function comprising 16 alternating blocks of rest and active conditions (8 for each condition). Each active block included 16 trials of 0.2s duration with 0.8s gap (Figure 1b). Random noise was added to achieve signal-to-noise ratio (SNR) levels of 50, 100 and 150 (Figure 1d). Noise was added without consideration of autocorrelation:

$$TC = TC \times (1 + \sigma \times randn), \quad (8)$$

where  $TC$  is the time course of simulated fMRI data;  $\sigma$  is the standard deviation (0.02, 0.01, and 0.067 for SNR of 50, 100, and 150, respectively); and the *randn* refers to a vector of pseudorandom values drawn from the standard normal distribution with the same length as  $TC$ . The range of SNR levels was selected given previous studies showing that the minimum SNR for detecting signal change in fMRI studies is 69 and the highest possible SNR is 154.<sup>21</sup> The simulated signal was sampled according to a typical fMRI acquisition with  $TR = 2.1s$  (Figure 1e). Each simulation was run 100 times.

### *HRF model selection*

HRF modeling was performed using an in-house MATLAB (MATLAB R2010a, The MathWorks Inc., Natick, MA) toolkit, sHRF, which is publicly available at our website (<http://www.cai.uq.edu.au/shrf-toolkit>). The fMRI time courses were high-pass filtered with a 128 s discrete cosine basis set and then fitted with the convolution of the HRF models (Table 1) and the stimulus function:<sup>22</sup>

$$TC = h(t) * u(t) + C \quad , \quad (8)$$

where  $h(t)$  and  $u(t)$  are the HRF and stimulus function, respectively. For the fitting we used a modified constrained Nelder-Mead Simplex algorithm that allows the use of constraints specified as parameter bounds (<http://www.mathworks.com/matlabcentral/fileexchange/8277>). Fitting was initialized using parameters which generated an initial HRF shape that closely matched that of the canonical HRF. Initial values and constraints for each model are summarized in Table 1. Parameter constraints were set empirically to cover plausible HRFs with the following characteristics: an initial dip with a minimum at 0-3s of magnitude 0-5%; peak BOLD signal at 2-10s of magnitude 0-15%; signal undershoot with a minimum

at 6-25s of magnitude 0-10%. The five models cover the same space of possible HRFs except where the functional form imposes a limitation in the ability to describe the HRF. For example, Model I covers the same space for the amplitude of the BOLD peak as other models but does not allow temporal variation; Model II covers the same space for the BOLD peak and undershoot as Models III – V but the functional form does not allow an initial dip. The parameter  $C$  allows baseline adjustment of the fitted time course to match that of the simulated time series (Figure 1d). The trueness of estimated HRF parameters or the closeness of agreement between measured and ground truth values was assessed by calculating the relative deviation from the values for the HRF used to generate the simulated fMRI time course, i.e. the difference between estimated and ground truth values divided by the ground truth value. The measure of precision, or relative uncertainty, used in this study was the inter-quartile range of relative deviation from the values for the HRF used to generate the simulated fMRI time course. Trueness and precision were summarized using boxplots of the simulation results created in MATLAB (MATLAB R2010a, The MathWorks Inc., Natick, MA). The identifiability of HRF models was assessed using their Akaike weights,<sup>23</sup> which is the probability of each model transformed from the Akaike Information Criterion (AIC):

$$w_i = e^{-\frac{1}{2}\Delta_i(AIC)} / \sum_{j=1}^M e^{-\frac{1}{2}\Delta_j(AIC)}, \quad \Delta_i(AIC) = AIC_i - \min(AIC) \quad (9)$$

in which  $M$  is number of models tested and  $\Delta_i(AIC)$  is the difference between the AIC of each model and that of model with the smallest AIC value. In this study, we used the AIC for finite samples:<sup>24</sup>

$$AIC = n \ln(RSS/n) + 2k(k+1)/(n-k-1) \quad (10)$$

where  $RSS$  is the residual sum of squares between the fitted and fMRI time courses,  $n$  is the sample size, and  $k$  is the number of parameters. The HRF model with the highest AIC weight was selected for subsequent analyses of parameter estimation and reproducibility.

#### *Parameter estimation from block design fMRI data*

The noise in measured fMRI time series and sparse sampling in acquired data may lead to HRF parameter mis-specification. To examine this, we used the balloon model simulation<sup>17, 18</sup> as the ground truth. The HRF parameters were varied in three ways: 1.  $H$  only, 2.  $T$  and  $O$  only, and 3.  $W$ ,  $T$ , and  $O$  only. As illustrated in Figure S2, varying  $T$  unavoidably changed  $O$  and varying  $W$  unavoidably changed  $T$  and  $O$ . The temporal SNR was set at 100, a typical SNR for fMRI data according to previous reports.<sup>25, 26</sup> The highest variability across subjects observed in the literature is 25%.<sup>1, 3, 19</sup> Hence, we varied ground truth HRF parameter values by 25%, 15% and 10%. The same simulation procedure was used as for model comparison except that only Model III was used. The simulation was executed 100 times for each type and level of parameter variation. The estimated HRF parameters were compared using the paired  $t$ -test in SPSS20 (IBM, New York).

#### *Variations in the block design paradigm*

To investigate the influence of variations in the block design paradigm on the trueness and precision of HRF modeling, the experimental conditions of the block design were systematically varied: 1. the number of blocks was varied from 1 block to 8 blocks in steps of 1 block; 2. block length was varied from 4s to 16s in steps of 2s; 3. stimulus duration was varied from 0.2s to 6.2s in steps of 1s and a stimulus duration of 16s in

individual blocks (long block design) was also evaluated; 4. the gap between individual stimuli in each block was varied from 0.8s to 6.8s in steps of 1s. Simulation of the fMRI time course was carried out as described above using the balloon model to generate ground truth, a SNR of 100 and Model III. Each simulation was executed 100 times. Trueness and precision for each paradigm were calculated as described above.

#### *Experimental fMRI time course data*

The data we analyzed were acquired as part of a prior fMRI study,<sup>11</sup> the Queensland Twin Imaging Study (QTIMS).<sup>27</sup> Retrospective utilization of the data was approved by the Research Ethics Committee of the Queensland Institute of Medical Research and The University of Queensland in compliance with the Australian National Statement on Ethical Conduct in Human Research. Functional MRI data from 30 male and 52 female healthy young adult twins of mean age  $22.5 \pm 2.5$  (Standard Deviation) years were included. For all participants, the fMRI scans were repeated 2-6 months later (mean  $117 \pm 56$  days).

Participants performed the 0- and 2-back versions of the N-back working memory task. The detailed fMRI experimental procedure is described in a previous report.<sup>28</sup> In the N-back task, a series of numbers is presented on a screen. The 0-back condition required participants to respond to the number currently shown on the screen. The 2-back condition required participants to respond to the number presented 2 trials earlier. The number was presented for 200 ms with an 800 ms interval between stimuli and 16 trials per block. In total, 16 alternating blocks were performed for the two conditions (8 blocks per condition).

The 3D T1-weighted MR image and echo planar imaging (EPI) data were acquired on a 4T Bruker Medspec whole body scanner (Bruker, Germany). 3D T1-weighted images were acquired using an MP-RAGE pulse sequence (TR = 2500 ms, TE = 3.83 ms, T1 = 1500 ms, flip angle = 15 degrees,  $0.89 \times 0.89 \times 0.89$  mm). For each participant, 127 sets of EPI data (TR = 2.1 s, TE = 30 ms, flip angle = 90,  $3.6 \times 3.6 \times 3.0$  mm) were acquired continuously during the tasks.

The fMRI data were analyzed using Statistical Parametric Mapping (SPM8, the Wellcome Trust Centre for Neuroimaging, London, UK). The first five EPI volumes were discarded to ensure that tissue magnetization had reached steady state. The spatial preprocessing included 2-pass motion correction<sup>29</sup> and spatial normalization to the average brain T1 template<sup>30</sup> implemented in SPM8. Normalized volumes were smoothed with an  $8 \times 8 \times 8$  mm full width half maximum Gaussian kernel. In a first level analysis of individual subject data, we determined locations of activation using the general linear model with a finite impulse response (FIR) basis function. The 2-back minus 0-back contrast images were then entered into a group-level, random-effects one-sample *t*-test to identify the common activation voxels ( $P < 0.05$  with family wise error rate adjustment for multiple comparisons).

Four regions identified at the group level were selected for HRF modeling: left and right middle frontal gyrus and left and right angular gyrus (Figure S3). Volumes of interest (VOIs) were defined as the overlap of an existing probabilistic atlas of each structure in stereotaxic coordinate space<sup>31</sup> with group activation regions. For each participant, the fMRI time course was extracted by averaging the signal intensity at

each time point in the voxels with the top 12.5% of SPM  $t$  statistics within each VOI. The top 12.5% is used here to accommodate individual variation in the pattern of functional activation within each VOI. The threshold was selected empirically as the value when the extracted time course stabilized as the percentage was decreased from 100%, 50%, 25%, to 12.5%. The HRF model selected from the simulation study was fitted to the extracted time series and used to estimate HRF parameters. AIC weights were also calculated for each HRF model using real time series data.

#### *Analysis of test-retest reliability*

For each brain region and each HRF parameter, the intra-class correlations (ICCs) of the two experimental sessions were calculated using SPSS20 (IBM, New York) using a two factor mixed effects model and tests of significant difference in ICC from zero performed.<sup>32</sup> Because the participants were biologically related monozygotic and dizygotic twins, the ICCs of the HRF heights from the first-born participant in each twin pair were also evaluated to assess whether relatedness between participants affected the reliability results. The reliability of the performance measure used in the experiment has been reported previously.<sup>11</sup>

## Results

### *Simulation study*

Figure 2 summarizes the HRF parameter estimates from the simulations. Parameter estimation was considered accurate if estimated values did not differ significantly (i.e.  $P > 0.05$ ) from the corresponding ground truth values.  $H$  was estimated accurately for all SNR levels and all models except for Model V at an SNR of 50 in simulation 1 ( $P < 0.05$ , one sample  $t$ -test). For Model I,  $T$ ,  $W$ , and  $O$  are fixed and there is only one free parameter. Models II, III, and IV were able to estimate  $T$ ,  $W$ , and  $O$  of the HRF for all noise levels accurately. Model V was able to estimate  $T$  and  $W$  accurately at all noise levels but did not estimate  $O$  accurately ( $P < 0.05$  for all 3 simulations). The central line and lower and upper box boundaries of the box plots in Figure 3 respectively represent the median, 25th and 75th percentiles of 100 simulations. Models with more free parameters showed a lower precision (wider range) of parameter estimation but higher trueness (smaller relative deviation) than those with fewer parameters. Model I had the least variation but the highest bias of parameter estimation. For all three simulations, the variation and bias of parameter estimation decreased with increasing SNR for all models. For Models II-V,  $T$  was estimated with the highest precision and trueness followed by  $W$ ,  $H$ , and  $O$ .

-----

Figure 2

-----

Table 2 summarizes the AIC of different models for data with different noise levels. Model III had the highest AIC weights and Model I the lowest across different simulations and noise levels.

-----

Table 2

-----

Results for HRF parameter estimation are summarized in Table 3. The selected HRF model (Model III) was able to identify parameter differences exceeding 10% with SNR of 100. There were no instances in which significant changes in one parameter resulted from variation in another parameter.

-----

Table 3

-----

Results of parameter estimation with different block design paradigms are summarized in Figure 3 using boxplots constructed in the same manner as Figure 2. For less than 6 blocks, mean estimated  $H$ ,  $W$ , and  $O$  generally had relative errors greater than 0.1 and an interquartile range greater than 0.5 (Figure 3a). Trueness was similar across paradigms with different block lengths. However, precision was increased with reduced block length (Figure 3b). Both trueness and precision of parameter estimation increased with greater stimulus duration within each block (Figure 3c). Trueness and precision also increased when the gap between stimuli was increased to 3.8s and remained similar with larger gaps (Figure 3d).

-----

Figure 3

-----

### *Real fMRI data*

AIC weights for the models using real fMRI data were consistent with results from simulations (Table 2). Model III had the highest AIC weights. Activation maps

between the two experimental sessions were highly reproducible (Figure S3). Quantitative assessment of the repeatability of the activation map between two experimental sessions has been reported previously.<sup>11</sup> The ICC(3,1) of HRF parameters estimated in the two experimental sessions using Model III are summarized in Table 4. *H* and *T* are highly reproducible, *W* is moderately reproducible and reproducibility of *O* is low. The 95% confidence intervals of all parameters overlap between the two experimental sessions. *H* is lower in session 2 than in session 1. A practice effect was also observed in the performance data.<sup>11</sup> Biological relatedness between participants did not affect reliability results. The ICCs of HRF heights from the first-born participant in each twin pair ( $N = 41$ ) for left and right MFG and left and right AG were 0.64 ( $P < 0.01$ ), 0.58 ( $P < 0.01$ ), 0.63 ( $P < 0.01$ ), and 0.64 ( $P < 0.01$ ), respectively.

-----  
Table 4  
-----

## **Discussion**

Modeling of the HRF using fMRI is a non-invasive method to investigate the brain's hemodynamic response to neuronal activation. In this study, we found that with block design fMRI paradigms, most HRF models were able to estimate HRF parameters except for Model V which had difficulty estimating onsets. The sum of two gamma functions with six free parameters had the greatest identifiability of the five models tested but the accuracy of parameter estimation varied with block design attributes. *H*, *T* and *W* were reproducible between two experimental sessions.

We used computer simulations with a known ground truth to assess the performance of the HRF models. In the simulations, Gaussian noise was added at each SNR level without consideration of autocorrelation. However, fMRI noise typically exhibits temporal dependence (autocorrelation), therefore, the SNR level is slightly lower than in practice. Parrish et al. demonstrated that a minimum SNR of 69 is required to detect a 1% BOLD signal change with 112 image volumes.<sup>21</sup> Our results were similar, showing that Models I-IV could estimate  $H$  accurately with a SNR of 50 and 122 image volumes. The simulation results for the five models showed that models with more free parameters had lower precision but higher trueness of HRF parameter estimation (Figure 3). The canonical HRF (Model I) had the least variance, but the estimated height was more likely to be biased. The trade-off between the number of parameters and precision and trueness motivated the use of AIC weights for model selection.

A key consideration in HRF model selection is the number and nature of *a priori* assumptions. Recently, Lindquist et al. assessed the performance of different HRF models for event-related designs in terms of bias, mis-specification and statistical power<sup>4</sup>. Seven models were compared: the canonical HRF, canonical HRF with temporal derivatives, canonical HRF with temporal and dispersion derivatives, FIR, smoothed FIR, sum of two gamma functions, and the sum of three inverse logit functions. The study suggested the sum of two gamma functions is not optimal for fitting noisy data from event-related studies and should only be used on regions where it is known that there is signal present<sup>4</sup>. Our study focused on HRF modeling using block design fMRI data in which signal is present. As illustrated in the simulation study (Figure 3), models with few assumptions are more flexible or may handle HRF

shapes with unexpected response behaviors more accurately than models with many fixed parameters. However, a greater number of free parameters may also lead to overfitting of noise, lowering precision. This may explain the relatively poor performance of Model V in our study. In Lindquist et al.,<sup>4</sup> superior performance for Model V compared to gamma function models for event-related designs that have a high HRF estimation efficiency<sup>8</sup> and high temporal resolution (TR=0.5s),<sup>4,15</sup> most likely reflects Model V's greater flexibility.<sup>4,15</sup> In contrast, in the present study of block designs with low estimation efficiency, prior knowledge implicitly encoded in the gamma function models constrained them from overfitting noisy data. We used AIC weights to judge model identifiability. The AIC is a measure of the relative goodness of fit of a statistical model compared to others, with a penalty given for using extra parameters.<sup>33</sup> The AIC with a correction for finite sample sizes was used in this study (Equation 10); the correction is minimized when the sample size is large.<sup>24</sup> Based on AIC values, Wagenmakers et al. further proposed Akaike weights, which may be directly interpreted as conditional probabilities for each model.<sup>23</sup> For example, an AIC weight of 0.41 for Model III with real data in our study indicates that this model has a 41% probability of being the best model of those tested. The AIC values of different models are consistent between the simulations and real fMRI data. The results suggest that the sum of two gamma functions with six parameters is the best HRF model when it is known that there is signal present. With a typical fMRI SNR of 100, a two gamma functions, 6 parameter model can discern 15% HRF feature variation without misattributing variation in one parameter to another. Inter- and intra-subject variability of the HRF has been studied previously in event-related fMRI experiments.<sup>1, 3, 19, 34-36</sup> In the present examination of a block design study,  $H$ ,  $T$ , and  $W$  were reproducible between two experimental sessions, supporting the validity

of these HRF parameters as biological measures. The repeatability results may also provide insight into neural responses and neurovascular coupling. For example, the reproducibility of  $H$  between trials implies that the neural firing rate as well as the vascular response induced by the same task across different sessions for each individual was very similar. In previous studies<sup>5, 37, 38</sup> the height of the BOLD response to visual stimulation was negatively correlated with resting GABA concentration in the visual cortex. If this relationship is widespread in the brain, our results suggest that endogenous factors, such as neurotransmitter concentration, which regulate the balance between excitation and inhibition in the individual brain may also remain relatively stable. The reproducibility of  $T$  and low reproducibility of  $O$  has implications for the ability to infer synchrony and directional influence among neural populations during task performance and in the resting state from block design fMRI data. Our findings on HRF test-retest reliability, particularly for temporal parameters, are in broad agreement with results from studies optimized for HRF estimation by the use of event-related designs and long baseline periods,<sup>1, 36</sup> in which time to peak had the greatest test-retest reliability and time when the BOLD response begins to rise steeply from baseline (similar to  $O$  in this study) had the largest test-retest variation. In this study, we represented neural activity by the stimulus time course, an assumption underlying commonly used methods for statistical parametric mapping. To the extent that this assumption is violated, it is likely that the HRF model parameters estimated here contain a component of neural activity in addition to vascular reactivity. Several techniques have been recently proposed to dynamically filter fMRI time courses in order to estimate neural activity as well as the vascular response explicitly.<sup>39, 40</sup> Application of these techniques in future studies may allow the reproducibility of the HRF to be estimated more specifically.

Many HRF models have been proposed in the literature. Our study was restricted to five models that are commonly used or have been shown in prior studies to be less susceptible to mis-specification errors (sum of inverse logit functions) or parameter bias (sum of two gamma functions). In this study, we examined vascular responses to neural activity evoked by a single cognitive function in four brain structures that demonstrated robust activation. Further studies using other activation tasks are needed to assess generalizability of our findings to other brain regions and brain functions.

Block designs are not optimal for HRF estimation and random event-related designs and m-sequence designs have been shown to have higher estimation efficiency.<sup>9</sup> Nonetheless, our data on model selection and on the reliability of HRF estimation should increase the utility of existing block design fMRI data. Indeed, the methodology presented in this paper will be used to analyze the heritability of HRF parameters in a large twin cohort using block design fMRI data that were originally collected to address heritability of spatial patterns of functional activation with a working memory task.<sup>11</sup> In our tests of the effects of varying the attributes of the block design paradigm, we found that at least 6 blocks are required to model the HRF accurately. The simulations showed that prolonging the length of blocks does not affect the trueness of the parameter estimation but decreases precision. This result is in keeping with HRF modeling being more sensitive to the initial increase and the final decrease of the signal than the plateau stages in the middle of block. Prolonging the block introduces additional noise reducing precision. Decreasing the frequency of stimuli in each block by increasing the gap between stimuli increases the accuracy of parameter estimation. This finding agrees with previous a theoretical model

describing the trade-off between estimation efficiency and detection power<sup>8</sup> in the sense that block designs with decreasing stimulus frequency in each block bear a greater resemblance to event-related designs.

In conclusion, we investigated trueness, precision, model identifiability and test-retest reproducibility of parameter estimates for HRF models with a block design paradigm using simulated and real fMRI data. The HRF features of height, time to peak, and width were reproducible between test sessions and may be useful as measures to characterize the coupled vascular response to neural activity in individual subjects.

#### **Disclosure/Conflict of Interest**

The authors declare no conflict of interest

**Supplementary information is available at the Journal of Cerebral Blood Flow & Metabolism website – [www.nature.com/jcbfm](http://www.nature.com/jcbfm)**

#### **Acknowledgements**

We thank the twins for participating in this study, research nurses Marlene Grace and Ann Eldridge at QIMR for twin recruitment, and radiographers Matthew Meredith, Peter Hobden, and Aiman Al Najjar from the Centre for Advanced Imaging, The University of Queensland, for data acquisition, and research assistants Kori Johnson and Lachlan Strike, Queensland Institute of Medical Research, for preparation and management of the imaging files. Data acquisition was supported by the Eunice Kennedy Shriver National Institute of Child Health & Human Development (Grant RO1HD050735) and National Health and Medical Research Council, Australia (Project Grant 496682).

## Figure Legends

**Figure 1.** The procedure used to simulate the fMRI signal time course. (a) A typical HRF generated using three gamma functions. Illustrated are the HRF parameters used to describe HRF shape: height ( $H$ ), time to peak ( $T$ ), full-width-at-half-maximum ( $W$ ), and onset ( $O$ ). (b) The stimulus function created according to a typical experimental design used in human fMRI experiments. (c) The signal time course generated by convolution of HRF and the stimulus function. (d) The signal time course after adding random noise. The average random variation of the signal was set to 50% of the true signal change.

**Figure 2.** Box-and-whisker plot of the relative differences of estimated HRF parameters from the true values in the simulation study. Outliers were defined as exceeding 3 times the standard deviation; all data including outliers were included in the analysis. Rows from top to bottom are the results for height ( $H$ ), time to peak ( $T$ ), width ( $W$ ), and onset ( $O$ ). Columns from left to right are results for Simulation 1 ('balloon' model), Simulation 2 (sum of four inverse logit functions) and Simulation 3 (sum of three gamma functions).

**Figure 3.** Box plots of estimated HRF features with systematic variation in attributes of the block design paradigm. The columns from left to right relate to estimated height, time-to-peak, width, and onset respectively. The rows from top to bottom relate to variation in the number of blocks (a), the length of blocks (b), the duration of stimuli in each block (c), and the gap between individual stimuli (d). Outliers were defined as exceeding 3 times the standard deviation. Outliers were not excluded from data analysis.

## References

1. Aguirre GK, Zarahn E, D'Esposito M. The variability of human, BOLD hemodynamic responses. *NeuroImage* 1998; 8: 360-369.
2. Bellgowan PSF, Saad ZS, Bandettini PA. Understanding neural system dynamics through task modulation and measurement of functional MRI amplitude, latency, and width. *Proc Natl Acad Sci USA* 2003; 100: 1415-1419.
3. Handwerker DA, Gonzalez-Castillo J, D'Esposito M, Bandettini PA. The continuing challenge of understanding and modeling hemodynamic variation in fMRI. *NeuroImage* 2012; 62: 1017-1023.
4. Lindquist MA, Loh JM, Atlas LY, Wager TD. Modeling the hemodynamic response function in fMRI: Efficiency, bias and mis-modeling. *NeuroImage* 2009; 45: S187-S198.
5. Muthukumaraswamy SD, Edden RAE, Jones DK, Swettenham JB, Singh KD. Resting GABA concentration predicts peak gamma frequency and fMRI amplitude in response to visual stimulation in humans. *Proc Natl Acad Sci USA* 2009; 106: 8356-8361.
6. D'Esposito M, Deouell LY, Gazzaley A. Alterations in the bold FMRI signal with ageing and disease: A challenge for neuroimaging. *Nat. Rev. Neurosci.* 2003; 4: 863-872.
7. Iadecola C. Neurovascular regulation in the normal brain and in Alzheimer's disease. *Nat. Rev. Neurosci.* 2004; 5: 347-360.
8. Liu TT, Frank LR, Wong EC, Buxton RB. Detection Power, Estimation Efficiency, and Predictability in Event-Related fMRI. *NeuroImage* 2001; 13: 759-773.
9. Maus B, van Breukelen GJP, Goebel R, Berger MPF. Optimal design for nonlinear estimation of the hemodynamic response function. *Human Brain Mapping* 2012; 33: 1253-1267.
10. Tahmasebi AM, Artiges E, Banaschewski T, Barker GJ, Bruhl R, Buechel C *et al.* Creating probabilistic maps of the face network in the adolescent brain: A multicentre functional MRI study. *Human Brain Mapping* 2012; 33: 938-957.
11. Blokland GAM, McMahon KL, Thompson PM, Martin NG, de Zubicaray GI, Wright MJ. Heritability of Working Memory Brain Activation. *Journal of Neuroscience* 2011; 31: 10882-10890.
12. Valsasina P, Rocca MA, Absinta M, Sormani MP, Mancini L, De Stefano N *et al.* A multicentre study of motor functional connectivity changes in patients with multiple sclerosis. *European Journal of Neuroscience* 2011; 33: 1256-1263.

13. Friedman L, Stern H, Brown GG, Mathalon DH, Turner J, Glover GH *et al.* Test-retest and between-site reliability in a multicenter fMRI study. *Human Brain Mapping* 2008; 29: 958-972.
14. Bonelli SB, Thompson PJ, Yogarajah M, Vollmar C, Powell RHW, Symms MR *et al.* Imaging language networks before and after anterior temporal lobe resection: Results of a longitudinal fMRI study. *Epilepsia* 2012; 53: 639-650.
15. Lindquist MA, Wager TD. Validity and power in hemodynamic response modeling: A comparison study and a new approach. *Human Brain Mapping* 2007; 28: 764-784.
16. van Zijl PCM, Hua J, Lu H. The BOLD post-stimulus undershoot, one of the most debated issues in fMRI. *NeuroImage* 2012; 62: 1092-1102.
17. Buxton RB, Frank LR, Wong EC, Siewert B, Warach S, Edelman RR. A general kinetic model for quantitative perfusion imaging with arterial spin labeling. *Magnetic Resonance in Medicine* 1998; 40: 383-396.
18. Friston KJ, Mechelli A, Turner R, Price CJ. Nonlinear responses in fMRI: The balloon model, volterra kernels, and other hemodynamics. *NeuroImage* 2000; 12: 466-477.
19. Handwerker DA, Ollinger JM, D'Esposito M. Variation of BOLD hemodynamic responses across subjects and brain regions and their effects on statistical analyses. *NeuroImage* 2004; 21: 1639-1651.
20. Logothetis NK, Pauls J, Augath M, Trinath T, Oeltermann A. Neurophysiological investigation of the basis of the fMRI signal. *Nature* 2001; 412: 150-157.
21. Parrish TB, Gitelman DR, LaBar KS, Mesulam MM. Impact of signal-to-noise on functional MRI. *Magnetic Resonance in Medicine* 2000; 44: 925-932.
22. Lagarias JC, Reeds JA, Wright MH, Wright PE. Convergence properties of the Nelder-Mead simplex method in low dimensions. *Siam Journal on Optimization* 1998; 9: 112-147.
23. Wagenmakers EJ, Farrell S. AIC model selection using Akaike weights. *Psychonomic Bulletin & Review* 2004; 11: 192-196.
24. Burnham KP, Anderson DR. Multimodel inference - understanding AIC and BIC in model selection. *Sociological Methods & Research* 2004; 33: 261-304.
25. Triantafyllou C, Hoge RD, Krueger G, Wiggins CJ, Potthast A, Wiggins GC *et al.* Comparison of physiological noise at 1.5 T, 3 T and 7 T and optimization of fMRI acquisition parameters. *NeuroImage* 2005; 26: 243-250.

26. Triantafyllou C, Polimeni JR, Wald LL. Physiological noise and signal-to-noise ratio in fMRI with multi-channel array coils. *NeuroImage* 2011; 55: 597-606.
27. de Zubicaray GI, Chiang M-C, McMahon KL, Shattuck DW, Toga AW, Martin NG *et al.* Meeting the Challenges of Neuroimaging Genetics. *Brain Imaging and Behavior* 2008; 2: 258-263.
28. Callicott JH, Ramsey NF, Tallent K, Bertolino A, Knable MB, Coppola R *et al.* Functional magnetic resonance imaging brain mapping in psychiatry: Methodological issues illustrated in a study of working memory in schizophrenia. *Neuropsychopharmacology* 1998; 18: 186-196.
29. Friston KJ, Frith CD, Turner R, Frackowiak RSJ. Characterizing evoked hemodynamics with fMRI. *NeuroImage* 1995; 2: 157-165.
30. Ashburner J, Friston KJ. Nonlinear spatial normalization using basis functions. *Human Brain Mapping* 1999; 7: 254-266.
31. Shattuck DW, Mirza M, Adisetiyo V, Hojatkashani C, Salamon G, Narr KL *et al.* Construction of a 3D probabilistic atlas of human cortical structures. *NeuroImage* 2008; 39: 1064-1080.
32. McGraw KO, Wong SP. Forming inferences about some intraclass correlations coefficients. *Psychological Methods* 1996; 1: 390-390.
33. Akaike H. New look at Statistical-model identification. *IEEE Transactions on Automatic Control* 1974; AC19: 716-723.
34. Birn RM, Saad ZS, Bandettini PA. Spatial heterogeneity of the nonlinear dynamics in the fMRI BOLD response. *NeuroImage* 2001; 14: 817-826.
35. McGonigle DJ, Howseman AM, Athwal BS, Friston KJ, Frackowiak RSJ, Holmes AP. Variability in fMRI: An examination of intersession differences. *NeuroImage* 2000; 11: 708-734.
36. Neumann J, Lohmann G, Zysset S, von Cramon DY. Within-subject variability of BOLD response dynamics. *NeuroImage* 2003; 19: 784-796.
37. Donahue MJ, Near J, Blicher JU, Jezzard P. Baseline GABA concentration and fMRI response. *NeuroImage* 2010; 53: 392-398.
38. Muthukumaraswamy SD, Evans CJ, Edden RAE, Wise RG, Singh KD. Individual variability in the shape and amplitude of the BOLD-HRF correlates with endogenous GABAergic inhibition. *Human Brain Mapping* 2012; 33: 455-65.
39. Friston KJ. Variational filtering. *NeuroImage* 2008; 41: 747-766.

40. Havlicek M, Friston KJ, Jan J, Brazdil M, Calhoun VD. Dynamic modeling of neuronal responses in fMRI using cubature Kalman filtering. *NeuroImage* 2011; 56: 2109-2128.

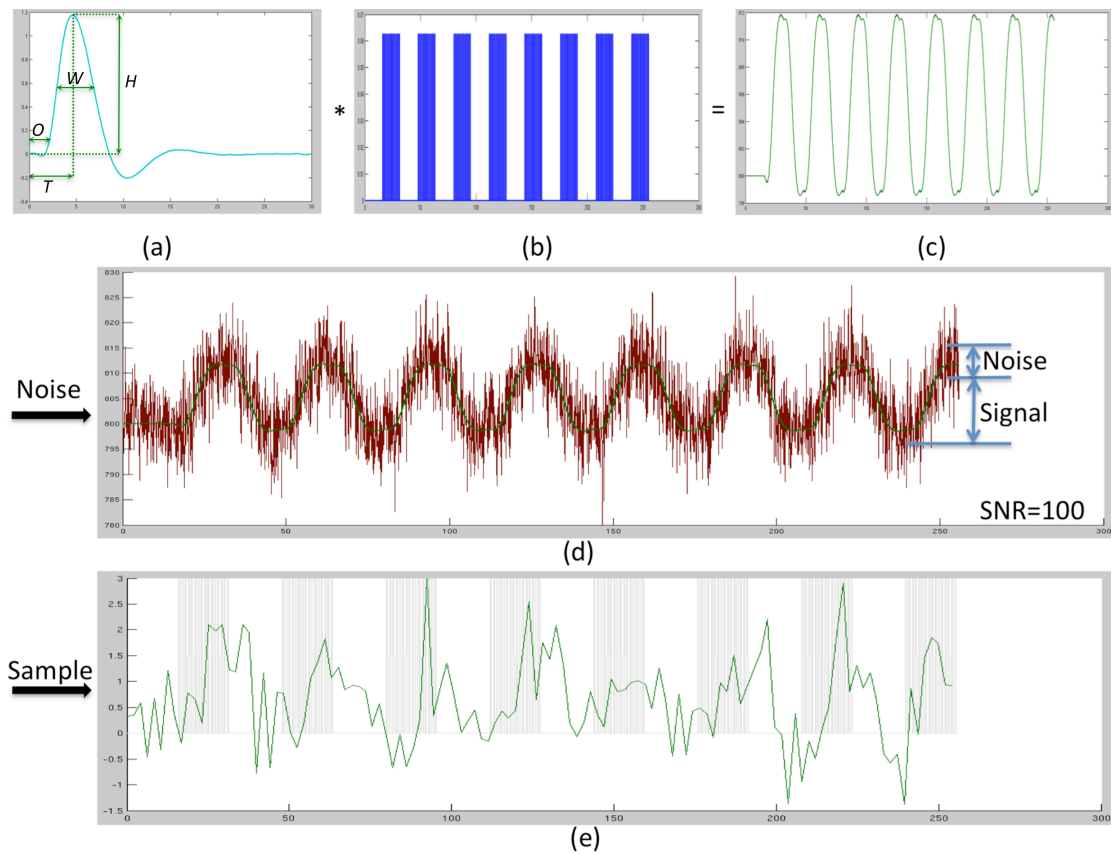


**Figure 1.** The procedure used to simulate the fMRI signal time course. (a) A typical HRF generated using three gamma functions. Illustrated are the HRF parameters used to describe HRF shape: height ( $H$ ), time to peak ( $T$ ), full-width-at-half-maximum ( $W$ ), and onset ( $O$ ). (b) The stimulus function created according to a typical experimental design used in human fMRI experiments. (c) The signal time course generated by convolution of HRF and the stimulus function. (d) The signal time course after adding random noise. The average random variation of the signal was set to 50% of the true signal change.

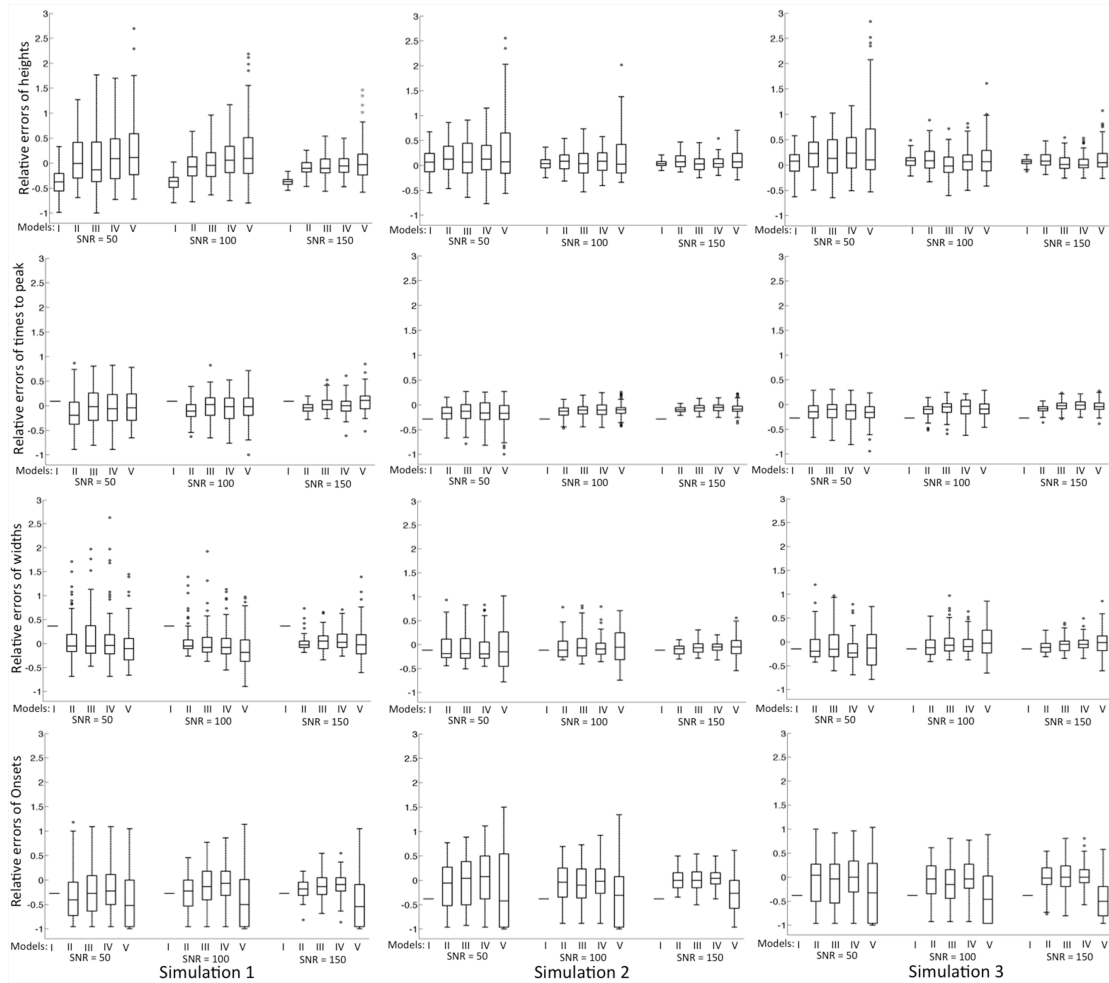


**Figure 2.** Box-and-whisker plot of the relative differences of estimated HRF parameters from the true values in the simulation study. Outliers were defined as exceeding 3 times the standard deviation; all data including outliers were included in the analysis. Rows from top to bottom are the results for height ( $H$ ), time to peak ( $T$ ), width ( $W$ ), and onset ( $O$ ). Columns from left to right are results for Simulation 1 (‘balloon’ model), Simulation 2 (sum of four inverse logit functions) and Simulation 3 (sum of three gamma functions).

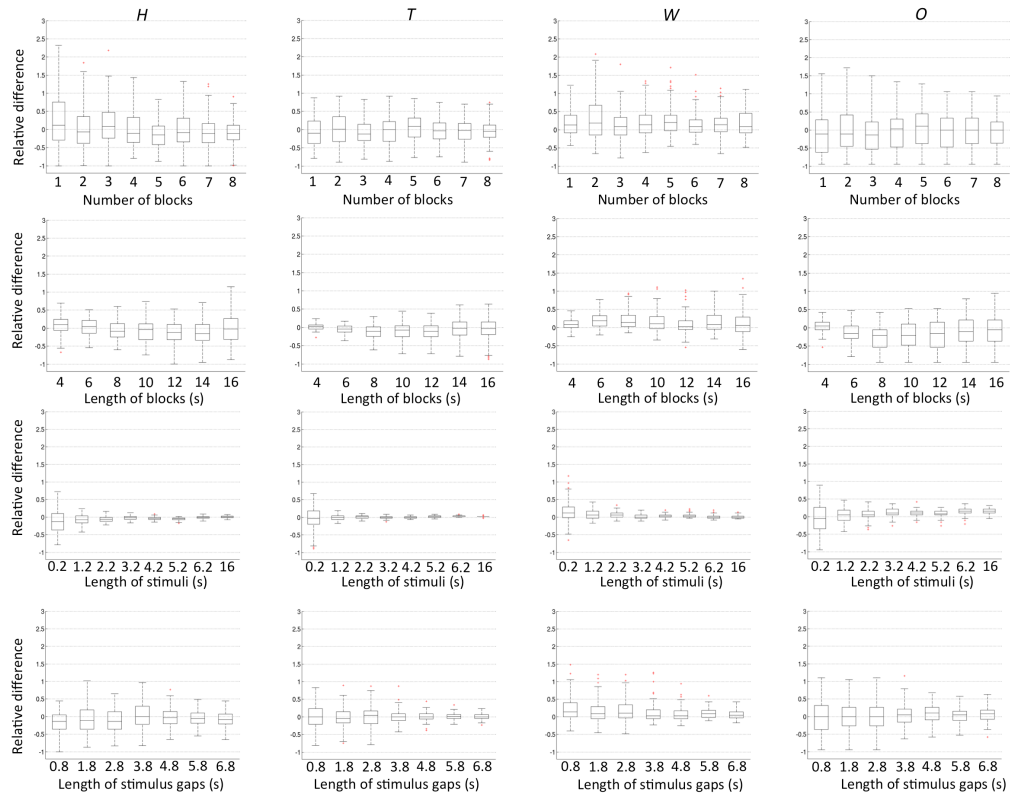


**Figure 3.** Box plots of estimated HRF features with systematic variation in attributes of the block design paradigm. The columns from left to right relate to estimated height, time-to-peak, width, and onset respectively. The rows from top to bottom relate to variation in the number of blocks (a), the length of blocks (b), the duration of stimuli in each block (c), and the gap between individual stimuli (d). Outliers were defined as exceeding 3 times the standard deviation. Outliers were not excluded from data analysis.

Table 1 Summary of HRFs<sup>§</sup>

M	Equations	$k$	$P_0$	Bounds (LB;UB)
I	$h(t) = A[\frac{t^5 e^{-t}}{\Gamma(6)} - \frac{1}{6} \frac{t^{15} e^{-t}}{\Gamma(16)}]$ (1)	1	$A_0 = 6$	A (0; 15)
II	$h(t) = A\left(\frac{t^{\alpha_1-1} \beta_1^{\alpha_1} e^{-\beta_1 t}}{\Gamma(\alpha_1)} - \frac{t^{\alpha_2-1} \beta_2^{\alpha_2} e^{-\beta_2 t}}{6\Gamma(\alpha_2)}\right)$ (2)	5	$A_0 = 6$ $\alpha_{1,0} = 7$ $\beta_{1,0} = 1$ $\alpha_{2,0} = 16$ $\beta_{2,0} = 1$	A (0; 15) $\alpha_1$ (2; 10) $\beta_1$ (0.5; 2) $\alpha_2$ (6; 25) $\beta_2$ (0; 1.5)
III	$h(t) = \sum_{i=1}^2 (A_i \frac{t^{\alpha_i-1} \beta_i^{\alpha_i} e^{-\beta_i t}}{\Gamma(\alpha_i)})$ (3)	6	$A_{1,0} = 6$ $\alpha_{1,0} = 7$ $\beta_{1,0} = 1$ $A_{2,0} = 1$ $\alpha_{2,0} = 16$ $\beta_{2,0} = 1$	$A_1$ (0; 15) $\alpha_1$ (2; 10) $\beta_1$ (0.5; 2) $A_2$ (0; 10) $\alpha_2$ (6; 25) $\beta_2$ (0; 1.5)
IV	$h(t) = \sum_{i=1}^3 (A_i \frac{t^{\alpha_i-1} \beta_i^{\alpha_i} e^{-\beta_i t}}{\Gamma(\alpha_i)})$ (4)	9	$A_{1,0} = 0.5$ $\alpha_{1,0} = 1.5$ $\beta_{1,0} = 0.8$ $A_{2,0} = 6$ $\alpha_{2,0} = 7$ $\beta_{2,0} = 1$ $A_{3,0} = 1$ $\alpha_{3,0} = 16$ $\beta_{3,0} = 1$	$A_1$ (0; 5) $\alpha_1$ (0; 3) $\beta_1$ (0.5; 2) $A_2$ (0; 15) $\alpha_2$ (2; 10) $\beta_2$ (0.5; 2) $A_3$ (0; 10) $\alpha_3$ (6; 25) $\beta_3$ (0; 1.5)
V	$h(t) = \sum_{i=1}^3 A_i \frac{1}{1 + e^{(t-T_i)/D_i}}$ (5)	7	$A_{1,0} = 1$ $T_{1,0} = 4$ $D_{1,0} = 1$ $T_{2,0} = 5$ $D_{2,0} = 1.5$ $T_{3,0} = 10$ $D_{3,0} = 2$	$A_1$ (0; 10) $T_1$ (0; 5) $D_1$ (0; 10) $T_2$ (3; 10) $D_2$ (0; 10) $T_3$ (6; 25) $D_3$ (0; 10)

§: M: models;  $k$ : the number of free parameters in the HRF models;  $P_0$ : initial values for model fittings;  $LB$ : lower bounds;  $UB$ : upper bounds;  $A$ : height;  $\Gamma$ : the gamma function;  $A_i$ ,  $\alpha_i$ ,  $\beta_i$ ,  $T_i$ , and  $D_i$  control the height and direction, shape, scale, shift center, and slope of the HRF respectively.

Table 2 Akaike weights ( $W_i$ ) for HRF models for computer simulations and real fMRI data<sup>§</sup>

HRF Model	Simulation 1			Simulation 2			Simulation 3			Real data
	150	100	50	150	100	50	150	100	50	
III (2 Gamma functions 6 parameters)	0.34	0.31	0.25	0.36	0.33	0.27	0.4	0.33	0.3	0.41
IV (3 Gamma functions 9 parameters)	0.27	0.23	0.2	0.34	0.22	0.22	0.32	0.25	0.22	0.36
II (2 Gamma functions 5 parameters)	0.22	0.21	0.23	0.25	0.3	0.23	0.26	0.26	0.23	0.16
V (3 Inverse logit functions 7 parameters)	0.16	0.2	0.2	0.05	0.15	0.21	0.02	0.15	0.18	0.07
I (Canonical function)	0.01	0.05	0.12	<0.01	<0.01	0.07	<0.01	0.01	0.07	<0.01

<sup>§</sup>: The Akaike weights were calculated for each model at a specific SNR level (150, 100, and 50) with different ground truth generation method (Simulation 1, 2 and 3) on simulation data and on real fMRI data. The simulation was run 100 times for each condition.

Table 3 Estimation of HRF parameter variation<sup>§</sup>

<i>P</i>	Estimated parameters ( $\pm$ SD) with variations in percentage									
	$\Delta = 0$	$\Delta H = 10$	$\Delta H = 15$	$\Delta H = 25$	$\Delta T = 10$ <i>O</i> = 18	$\Delta T = 15$ <i>O</i> = 32	$\Delta T = 25$ <i>O</i> = 50	$\Delta W = 10$ $\Delta T = 9$	$\Delta W = 15$ $\Delta T = 13$ <i>O</i> = 4	$\Delta W = 25$ $\Delta T = 20$ <i>O</i> = 4
<i>H</i> (%)	1.12 $\pm$ 0.46	1.21 $\pm$ 0.49	1.31 $\pm$ 0.32*	1.41 $\pm$ 0.38**	1.14 $\pm$ 0.39	1.06 $\pm$ 0.39	1.11 $\pm$ 0.37	1.13 $\pm$ 0.45	1.17 $\pm$ 0.39	1.18 $\pm$ 0.35
<i>T</i> (s)	4.70 $\pm$ 0.92	4.65 $\pm$ 0.91	4.71 $\pm$ 0.78	4.45 $\pm$ 0.65	5.08 $\pm$ 0.81*	5.53 $\pm$ 0.75**	5.82 $\pm$ 0.68**	5.14 $\pm$ 0.93*	5.14 $\pm$ 0.84*	5.35 $\pm$ 0.85**
<i>W</i> (s)	3.85 $\pm$ 1.07	4.05 $\pm$ 1.07	4.10 $\pm$ 0.96	4.00 $\pm$ 0.98	4.08 $\pm$ 1.01	4.23 $\pm$ 1.25	4.15 $\pm$ 0.73	4.53 $\pm$ 1.09**	4.51 $\pm$ 1.01**	4.77 $\pm$ 0.97*
<i>O</i> (s)	1.90 $\pm$ 0.88	1.79 $\pm$ 0.84	1.83 $\pm$ 0.74	1.74 $\pm$ 0.82	2.20 $\pm$ 0.90	2.41 $\pm$ 0.85*	2.79 $\pm$ 0.89*	1.98 $\pm$ 0.81	2.02 $\pm$ 0.89	2.08 $\pm$ 0.89*

<sup>§</sup>: *P*, HRF parameters; *H*, height; *T*, time to peak; *W*, width; *O*, onset;  $\Delta$ , variation (no variation is introduced if  $\Delta = 0$  or the parameter is absent). The \* and \*\* denote  $P < 0.05$  and  $P < 0.001$ , respectively.

Table 4. The ICC(3,1) of HRF parameters between the two experimental sessions<sup>§</sup>

Structures	Parameters			
	Height	Time to peak	Width	Onsets
L-MFG	0.6** (1.23, 1.56; 1.03, 1.26)	0.53** (3.57, 4.09; 3.73, 4.21)	0.56** (3.49, 4.08; 3.84, 4.27)	0.22 (1.17, 1.5; 1.21, 1.49)
R-MFG	0.52** (1.21, 1.52; 1.05, 1.28)	0.5* (3.7, 4.29; 3.94, 4.52)	0.45* (3.75, 4.39; 4.26, 5.08)	0 (1.22, 1.54; 1.23, 1.59)
L-AG	0.74** (1.28, 1.56; 1.02, 1.29)	0.7** (3.66, 4.19; 3.78, 4.35)	0.48* (3.75, 4.27; 3.91, 4.74)	0.25 (1.18, 1.49; 1.24, 1.57)
R-AG	0.6** (1.12, 1.37; 1.02, 1.26)	0.45** (3.68, 4.29; 3.8, 4.43)	0.33* (4.02, 4.74; 4.28, 4.91)	0.42* (1.12, 1.47; 1.15, 1.59)

§: L-: left, R-: right, MFG: middle frontal gyrus, AG: angular gyrus, \*:  $P \leq 0.05$  and \*\*:  $P < 0.001$ . The numbers in the parentheses are the 95% confidence interval of the parameters (session 1 lower bound, session 1 upper bound; session 2 lower bound, session 2 upper bound)